A LETTERS JOURNAL EXPLORING THE FRONTIERS OF PHYSICS

OFFPRINT

Liquefaction of immersed granular media under isotropic compression

T. Doanh, A. Le Bot, N. Abdelmoula, S. Hans and C. Boutin

EPL, **108** (2014) 24004

OVER
560,000
full text downloads in 2013

24 DAYS
average accept to online publication in 2013

10,755
citations in 2013

"We greatly appreciate the efficient, professional and rapid processing of our paper by your team."

Cong Lin
Shanghai University

Six good reasons to publish with EPL

We want to work with you to gain recognition for your research through worldwide visibility and high citations. As an EPL author, you will benefit from:

1. **Quality** – The 50+ Co-editors, who are experts in their field, oversee the entire peer-review process, from selection of the referees to making all final acceptance decisions.
2. **Convenience** – Easy to access compilations of recent articles in specific narrow fields available on the website.
3. **Speed of processing** – We aim to provide you with a quick and efficient service; the median time from submission to online publication is under 100 days.
4. **High visibility** – Strong promotion and visibility through material available at over 300 events annually, distributed via e-mail, and targeted mailshot newsletters.
5. **International reach** – Over 2600 institutions have access to EPL, enabling your work to be read by your peers in 90 countries.
6. **Open access** – Articles are offered open access for a one-off author payment; green open access on all others with a 12-month embargo.

Details on preparing, submitting and tracking the progress of your manuscript from submission to acceptance are available on the EPL submission website **www.epletters.net**.

If you would like further information about our author service or EPL in general, please visit **www.epljournal.org** or e-mail us at **info@epljournal.org**.

EPL is published in partnership with:

European Physical Society | Società Italiana di Fisica | EDP Sciences | IOP Publishing

epl A Letters Journal Exploring the Frontiers of Physics

October 2014

EPL, **108** (2014) 24004 www.epljournal.org
doi: 10.1209/0295-5075/108/24004

Liquefaction of immersed granular media under isotropic compression

T. Doanh[1,2], A. Le Bot[2], N. Abdelmoula[1], S. Hans[1] and C. Boutin[1]

[1] *Ecole Nationale des Travaux Publics de l'Etat, LGCB, LTDS (UMR 5513) - Vaulx en Velin, France*
[2] *Ecole Centrale de Lyon, LTDS (UMR 5513) - Ecully, France*

received 18 June 2014; accepted in final form 7 October 2014
published online 24 October 2014

PACS 45.70.Cc – Granular systems: Static sandpiles; granular compaction
PACS 83.80.Fg – Rheology: Granular solids
PACS 83.85.St – Rheology: Stress relaxation

Abstract – We report an observation of the spontaneous liquefaction of glass beads immersed in water and compacted by external isotropic stress. We show that during compression, loose granular samples exhibit a series of sudden rearrangements accompanied by a transient overpressure of interstitial fluid. Ultimately, spontaneous liquefaction with large deformation of the sample is observed. By contrast, denser samples do not show a liquefaction by maintaining its shape integrity. We then discuss the potential mechanisms which could explain this unexpected liquefaction.

Introduction. – Liquefaction of immersed granular media as observed in geophysical situations is manifested by a loss of shearing resistance that results in catastrophic consequences. The most impressive example is certainly buildings sinking into the soil during an earthquake event. Even liquefaction is sometimes proposed as the triggering mechanism of earthquake [1]. Qualitatively, from the mechanical point of view, liquefaction of a granular packing immersed into water may be explained by a loss of contact of the grains. The grains float and are free to move and the medium behaves like a suspension that cannot support a heavy object. If U denotes the pressure in the interstitial water (pore pressure) and σ the confining pressure of the medium (external total stress), then liquefaction is synonymous to the vanishing of the effective stress $\sigma' = \sigma - U$ interpreted as the contact stress between grains formulated by Terzaghi [2]. Up to now, liquefaction has been observed in laboratory almost exclusively for totally saturated and loose granular materials (contracting) compressed by external *anisotropic* stress when the internal fluid is *undrained* [3]. For a contracting granular soil under undrained condition (null volumetric variation), an increase of external stress in one direction, say $\Delta\sigma_{11} > 0$, implies an increase of pore pressure $\Delta U > 0$. But in other directions for which the external stress does not vary, $\Delta\sigma_{22} = 0$, this variation of internal pore pressure is compensated by a negative variation of effective stress, $\Delta\sigma'_{22} + \Delta U = 0$ (Terzaghi) which ultimately leads to liquefaction. In nature, the shearing force can be imposed either by monotonic loading (*e.g.* static overload by man-made construction on soil) or cyclic loading (*e.g.* dynamic earthquake event) [4]. However, if the pore pressure is maintained constant, $\Delta U = 0$ (drained condition), an excess of external stress $\Delta\sigma > 0$ cannot give a reduction of effective stress. This is why liquefaction is *a priori* not possible when compacting in drained condition. We will show in this letter that this assessment does not always apply.

In the present work, we report that spontaneous compaction and ultimately liquefaction can be induced by *isotropic* compression in *drained* condition, *i.e.* with no excess pore pressure, on a fully saturated loose model granular assembly. Two basic ingredients are required to perform this simple and conceptually improbable experiment: a loose state of monodispersed model granular material and an initial structural anisotropic state. The isotropic external stress induces an anisotropic deformation of the sample leading to an internal rearrangement of the grain structure. Sometimes, catastrophic events arrive and cause a transient excess pore pressure. Although the internal fluid is nominally maintained at a constant pressure, the short-lived excess pore pressure may reach the effective stress in which case liquefaction is observed.

Experimental setup. – The experiment shown in fig. 1 consists in an isotropic drained compression of a

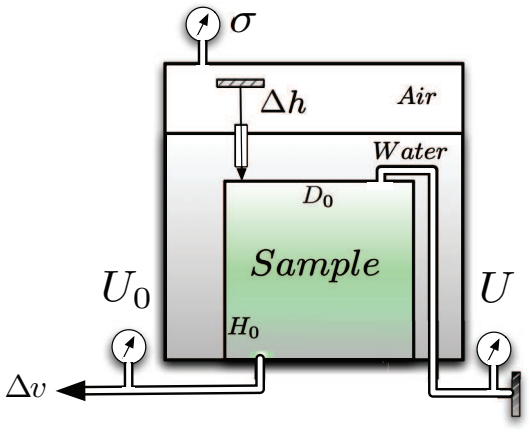

Fig. 1: (Color online) Sketch of the experimental setup for isotropic compression of a short cylindrical granular sample inside a triaxial cell.

short cylindrical granular sample inside a triaxial cell. The granular sample made of monodisperse and spherical soda lime glass beads (Sil-glass by CVP) of 0.723 mm mean diameter has very loose porosity, is fully saturated and was placed inside a triaxial cell at controlled pressure σ. The sample was enclosed inside a cylindrical and open-ended latex membrane of 0.3 mm thickness.

During compression, the water volume Δv expelled from or moving into the sample was measured (Wykeham Farrance, WF17038) and the global volumetric strain deduced from $\varepsilon_v = \Delta v/V_0$, where V_0 is the initial sample volume. The axial displacement Δh was measured by a linear variable differential transformer sensor (Chauvin Arnoux, L20) mounted directly on the top platen. The global axial strain is estimated from $\varepsilon_a = \Delta h/H_0$ with H_0 the initial height. The back pressure U_0 needed for a full saturation was applied at the bottom of the sample. The pore-water pressure U was recorded by a transducer (Kistler, MD20) outside the triaxial cell using a very thick plastic tube connected to the top cap of the granular sample, at a distance of about 60 cm. In static condition, $U = U_0$ is the homogeneous pore pressure. A synchronized acquisition system (HP3566A) was used to collect the data from different sensors.

The sample, $H_0 = 70$ mm in height and $D_0 = 70$ mm in diameter, was prepared using a modified moist tamping and under compaction method [5,6]. Predetermined quantities of moist glass beads, mixed with 2% of distilled water in weight, were placed and gently compacted in five layers of prescribed thickness using a flat-bottom circular stainless-steel tamper 20 mm in diameter. To obtain a fully saturated state, we used the CO_2 method [7] with deaired distilled water, and a constant back pressure U_0 of up to 200 kPa was applied. Prior to each experiment, we increased the net total stress $\Delta\sigma = \sigma - U_0$ and measured the excess pore pressure $\Delta U = U - U_0$ in undrained condition. The resulting Skempton's coefficient $B = \Delta U/\Delta\sigma \geq 0.95$ indicates a fully saturated sample [8]. The solid fraction Φ_{30} defined as the volume of solids of the granular sample to the total volume at confining pressure of 30 kPa was carefully evaluated from the water content obtained at the end of the isotropic compression [9], and also from the usual procedure of measuring the sample dimensions during different fabrication stages. To avoid possible wearing effects, only virgin glass beads were used.

During the isotropic drained compression test, σ was manually imposed using compressed air and slowly increased while keeping ΔU below 4–5 kPa to respect the requirement of full drainage.

Results. – A typical compressibility of very loose model granular materials is shown in fig. 2(a) which represents the evolution of solid fraction $\Phi = \Phi_{30}/(1 - \varepsilon_v)$ *vs.* total stress σ. Under imposed external stress, granular media such as sand, exhibit a continuous increase of density [3]. But in our experiments, instead of the expected smooth and continuous compaction, large unexpected drops in Φ can be seen. Between two events, the normal continuous increase of solid fraction is observed during the loading phase. No drop in Φ has been noticed in unloading.

However, the compressibility of the granular skeleton is revealed by introducing the effective stress $\sigma' = \sigma - U$ in fig. 2(b), with U the actual measured pore pressure. The drops A, B, C occur successively at effective stress ${\sigma'}_{trig}$ of 51, 80 and 267 kPa, respectively. Each event consists in a sudden and simultaneous compressive volumetric strain (compaction), together with a reduction of σ' due to a sudden surge of ΔU, followed by a gradual recover of σ'.

The complete individual time evolution of ΔU for the three events, ε_v and ε_a only for event C is plotted in fig. 3. The excess pore pressure ΔU was normalized by the brief stable value ΔU_{stable} between the oscillations and the return to equilibrium $\Delta U = 0$. The time origin is shifted to the beginning of the transient phase ± 0.5 ms, which is the current time resolution.

The evolution of ΔU can be decomposed in three phases. First a fast transient phase I (hollow circle in fig. 2(b)) occurred within 200 ms at constant volume and constant axial strain. ΔU vibrates like an oscillating underdamped system with a dominant frequency of 110 Hz (fig. 3). The rising time to the first peak ΔU_{max} is within 5 ms, followed by relatively fast decay to stabilizing ΔU_{stable}. Then an intermediate second phase II happened only for event C. It is chacracterized by a large increase of volumetric compaction (fig. 2(b)) and axial contraction (fig. 3) at constant σ' and at stabilizing value of ΔU_{stable} of the excess pore pressure. Finally a third and longest phase III in which ΔU returns to the initial equilibrium $U = U_0$ at nearly constant axial strain. During the transient phase I of all collapses, the sample briefly experiences negative values of σ'. The solid circles indicate the null effective stress levels. Nevertheless, the duration of this phase was not long enough to sustain a liquefaction state except for event C.

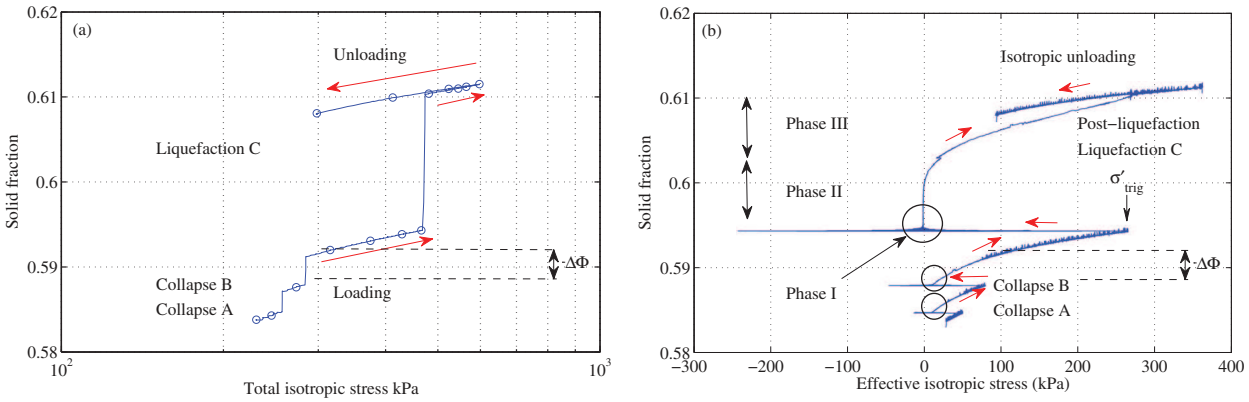

Fig. 2: (Color online) (a) Solid fraction *vs.* total isotropic stress. (b) Solid fraction *vs.* effective isotropic stress. Spontaneous collapses and liquefaction under isotropic compression from 30 to 400 kPa with $\Phi_{30} = 0.584$.

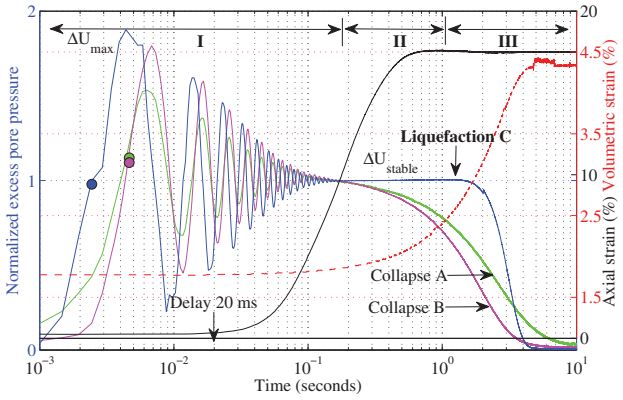

Fig. 3: (Color online) Three phases of pore water pressure development. I: fast and transient development, II: constant stable (liquefaction) value and III: dissipation (post-liquefaction). The axial strain (black) and volumetric strain (red) refer to the liquefaction event. Referred liquefaction levels (solid circles) are indicated.

The small increase of Φ for the first two events A and B did not compromise the cylindrical form of the specimen and permits the continuation of isotropic compression; hence, these events are terms as local collapses. In contrast, the last event C destroyed it with a much larger volumetric compaction, and the granular sample collapsed instantaneously onto the pedestal base of the triaxial cell in a spontaneous liquefaction or global collapse with a very large axial strain. For completeness, the isotropic compression was continued until 400 kPa for the post-liquefaction stage and the isotropic unloading afterwards to 100 kPa.

To check that the transient vibration is not an artifact of the measurement system, a dynamic pore pressure sensor (PCB S112A21) having high resonant frequency (250 kHz) was used together with the static one. No difference was detected. Since the pore pressure transducer is on the other side of the porous bronze disk of the top cap and far from the possibly triggering source inside the sample, the actual value of these sharp peaks is likely a minimum estimate.

The time evolution of ε_a for the catastrophic event C in fig. 3 reveals a fast axial contraction, after a small delay of about 20 ms with respect to ΔU, up to 17.60% from 0.27% within only 0.5 second. This vertical compression indicates an axial strain rate $\dot{\varepsilon_a}$ of about 35%/s, much faster than the usual constant $\dot{\varepsilon_a}$ of 0.0048%/s in triaxial drained compression experiment on sand. It clearly indicates a dynamic regime of the liquefaction phenomenon happening within less than one second. Note that half of the axial contraction already happens during the transient phase I of 200 ms, essentially under undrained conditions of $\varepsilon_v \approx 0$.

The volumetric strain indicates an overall compaction of only 2.56% during liquefaction, with a larger initial time delay and its development is far behind that of axial strain, both in terms of time evolution and magnitude. Figure 4 shows the complete evolution of U, σ, ε_a and ε_v for the total test duration. Manual control of total stress results in stepwise linear loading and unloading. The three events are shown here with a sudden and simultaneous drop of ε_v and ε_a at the beginning of each event. The three narrow and surprisingly very sharp peaks of U are clearly related to these events, despite the drainage system with porous bronze disk embedded in the end plates, and indicate a quite fast dissipation. The last peak, well above 400 kPa, was much larger than the two previous ones of about only 250 kPa and presumably responsible for the observed catastrophic liquefaction with a very large runaway $\Delta\varepsilon_a$ of more than 17% and a sudden volumetric compaction of 2.5% in less than one second.

Compressibility and anisotropy. – In fig. 5, the three loading phases preceding the collapse event (30–51 kPa before event A, 51–80 kPa before B and 80–267 kPa before C) are retrieved and artificially shifting downwards at σ'_{trig} by $\Delta\Phi$ from fig. 2 to form a continuous curve. For clarity, phases I and II are removed. The post-liquefaction and the isotropic unloading phases

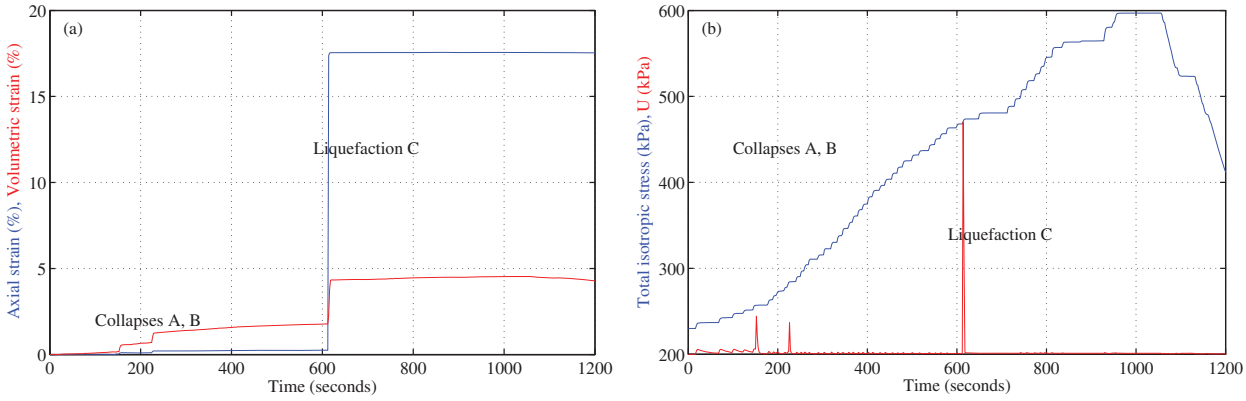

Fig. 4: (Color online) Time evolution of (a) axial strain ε_a and volumetric strain ε_v, (b) total isotropic stress σ and pore pressure U under isotropic compression from 230 to 600 kPa of total stress.

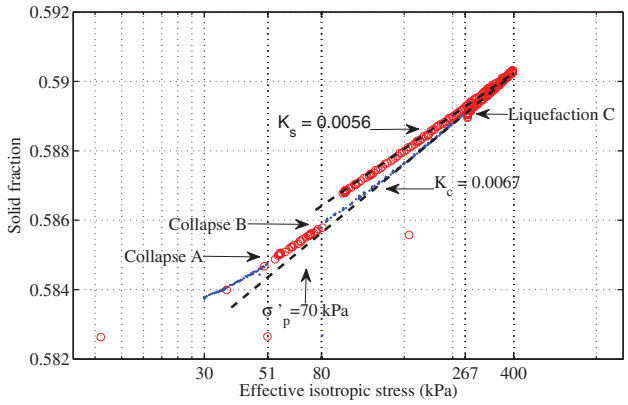

Fig. 5: (Color online) Compressibility parameters under isotropic compression, upon ignoring the void ratio reduction due to collapses and liquefaction. Alternate colors indicate successive sections of isotropic loading and unloading.

also appear. This construction reveals a hypothetical mechanical behaviour conforming to the usual isotropic compressibility of loose sand materials without unloading under fully drained conditions [10], or powders in uniaxial compression [11]. The compressibility behaviour can be approximated by two superimposed straight dashed lines in fig. 5 representing the normal compression line and the unloading-reloading line. The initial slope of the curve is usually lower but has the same value as the unloading line. The intersection point of these two lines defines the pre-compression stress σ'_p as a reminder of the past maximum effective stress.

Some macroscopic compressibility parameters can be identified: a compression index $K_c = \Delta\Phi/\Delta \log \sigma' = 0.0067$ of the loading line, a swelling index $K_s = \Delta\Phi/\Delta \log \sigma' = 0.0056$ of the unloading line, and a pre-compression stress $\sigma'_p = 70$ kPa which results from the under-compaction method. Loosely bound glass beads have a particular nearly elastic behaviour with $K_s \approx K_c$, in contrast with real granular materials [10] where $K_s \approx K_c/10$. This observation confirms the quasi-reversibility behaviour for model granular materials numerically obtained in [12], however, without the unexpected collapses and liquefaction.

Furthermore, the measurements of ε_v and ε_a during each segment preceding a local collapse have been systematically exploited to estimate the incremental anisotropy coefficient $i = \Delta\varepsilon_v/\Delta\varepsilon_a$. The typical value obtained before the last collapse is of about 16, indicating a highly anisotropic structure, contrasting sharply the isotropic structure $i \approx 3.0$ for loose laboratory sands (*i.e.* Hostun or Toyoura) created by the same moist-tamping procedure [13]. We deduce that this structural anisotropy can be a primary key element in fostering the observed liquefaction.

Random liquefaction and instabilities. – The occurrence of triggering stress σ'_{trig} is randomly distributed over a wide range. In the studied range from 30 to 500 kPa, it can be as small as 33 kPa without any preceding local collapses, or as large as 497 kPa with numerous preceding local collapses or precursors. In all tested samples, no more than 4 local collapses were observed before the final liquefaction.

Figure 6 shows the measured transient ΔU_{max} and ΔU_{stable} *vs.* σ'_{trig} for all events. ΔU_{max} (hollow symbols) is largely and briefly located above the diagonal red line representing the state of null effective stress where the excess pore pressure ΔU equals the net total stress $\Delta\sigma$. It can be speculated that most often the brief duration of ΔU_{max} in the range of 200 ms is enough to initiate local liquefaction but not enough to maintain its development and to propagate onto the whole sample. The stabilized values ΔU_{stable} (solid symbols) for all local collapses (square) are below or near this line; but those of the largest events (circle) are precisely on this line for a more lengthy time of at least one second. During this long time (phase II), the effective stress is null which is enough to develop and sustain liquefaction to the overall sample.

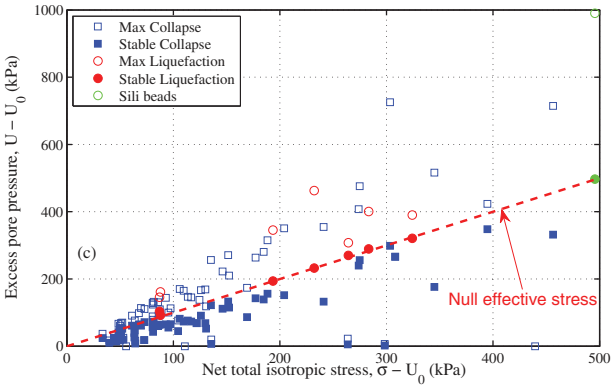

Fig. 6: (Color online) Effects of $\sigma'_{trig} = \sigma - U_0$ on the excess pore pressure in isotropic collapses and liquefaction. Hollow symbols indicate the maximum value ΔU_{max} (phase I) and solid symbols the stabilized value ΔU_{stable} (phase II).

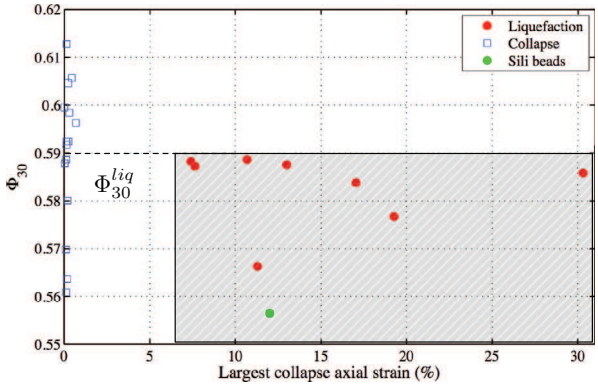

Fig. 7: (Color online) Identification of the threshold solid fraction Φ_{30}^{liq} indicating a total disappearance of liquefaction on denser samples.

A practical consequence is the impossibility to control the solid fraction increase under isotropic compression of very loose and moist-tamped model granular materials, due to the random occurrence of the dynamic instabilities, unless mastering the triggering mechanisms.

Threshold fabric solid fraction. – By repeating the experiments with samples of various solid fractions at the fabrication state, hence indirectly Φ_{30}, fig. 7 shows the total disappearance of full liquefaction, characterized by a sudden large axial contraction ($\varepsilon_a > 7\%$), of denser samples above a threshold solid fraction which can be narrowed down to $0.589 \leq \Phi_{30}^{liq} \leq 0.592$. This threshold solid fraction Φ_{30}^{liq} represents the transitional behaviour from full liquefaction (global collase) in isotropic compression to non-liquefaction with the presence of local collapses. It can be related to another known threshold solid fraction $\Phi_c \approx 0.516$–0.517, guaranteeing a liquefaction-free behaviour during subsequent undrained shearing for very loose Toyoura sand [9,14]. Φ_c represents the transition from liquefaction behaviour in undrained shearing to non-liquefaction behaviour characterized by the steady state of deformation [15]. However, local collapses can still be observed in isotropic loading.

Repeatability and other materials. – Despite a large number of tests on soda lime glass beads, only 8 samples have liquefied out of more than 80 experiments. However, all tests presented instabilities. Although being rare, isotropic liquefaction has been repeatedly and consistently observed in two years of work experience.

Liquefaction has also been observed with other glass beads of different chemical composition and different industrial fabrication processes (Sili beads by Sigmund-Lindner). These beads have a more symmetrical distribution in size than CVP and centered on smaller mean diameter of 0.675 mm. They are also less rounded. The results are shown in green symbols in figs. 6 and 7.

Macropore hypothesis. – Very loose glass bead samples created by moist tamping technique tend to have more irregular microstructures with the presence of macropores (cell of approximately fixed size constituted by aggregated grains surrounding a large pore), based on direct microscopic observations [16] on Hostun sand using the same fabrication technique. It is well known that the applied external forces were transmitted through the interparticle contact force network within granular media [17]. We speculate that under external isotropic pressure, the induced strain can be strongly anisotropic due to the initial structural anisotropy of the sample ($i \geq 16$) despite the observed quasi-elastic behaviour. The force chains (thick dashed lines in fig. 8 (left)) are therefore deformed and such fragile and anisotropic structures can be broken. The resulting ejection of one or more grains of the metastable honeycombed structures in fig. 8 (right) might be the mechanism responsible for the collapse phase. The incompressibility of the pore water and the spherical grain shape probably facilitate the failures of already fragile contact chain forces and this ejection. The remaining grains still form a new metastable structure and the ejected grains in the fully saturated media transmit the ejecting force into the pore fluid, hence briefly raise the pore pressure to ΔU_{max} and reduced later to ΔU_{stable}. Consequently, this very fast and strong build-up of ΔU reduces the effective stress and favors the instability, without triggering it. The rapid structural rearrangement can lead to a fast and irreversible volumetric compaction and axial contraction [18]. The local or global failure of the anisotropic contact network would explain the larger magnitudes of the collapse during the slip phase of the stick-slip phenomenon in saturated samples [19], compared to dry ones [20,21] in triaxial experiments; and the spontaneity of slip events in the experimental [22–24], or theoretical perspective [25].

It is worth noting that in all these experiments, no doublet of welded grains was found in binocular microscopy after testing.

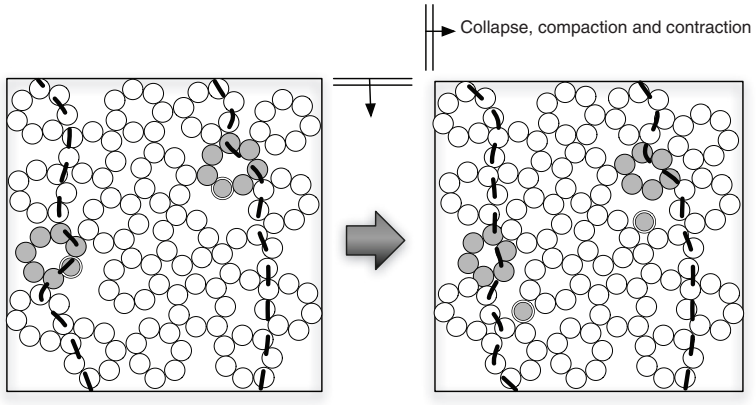

Fig. 8: Macropore hypothesis for loose model granular assembly.

Conclusions. – We reported the spontaneous liquefaction under isotropic drained compression of model granular materials and reveal some mechanisms underlying the diffuse instability phenomenon, usually hidden or partially developed in sands. The unexpected behaviour can offer some new insights into the complexity of granular matter; however to fully characterize the material response, one needs to understand how the excess pore pressure is initiated, propagated, maintained and ultimately causes liquefaction. The observed collapsible behaviour is currently difficult to predict within the framework of classical soil mechanics. It also represents a challenge for discrete element modelling where the solid-fluid interaction, the dynamic character of liquefaction as well as the creation of very loose granular assembly are still not fully implemented.

* * *

We wish to thank Julien Scheibert for fruitful discussions.

REFERENCES

[1] Johnson P. A. and Jia X., *Nature*, **437** (2005) 871.
[2] Terzaghi K., Peck R. P. and Mesri G., *Soil Mechanics in Engineering Practice*, 3rd edition (John Wiley) 1996.
[3] Andreotti B., Forterre Y. and Pouliquen O., *Granular Media: Between Fluid and Solid* (Cambridge University Press) 2013.
[4] Ishihara K., *Soil Behaviour in Earthquake Geotechnics* (Oxford University Press) 1996.
[5] Bjerrum L., Krimgstad S. and Kummeneje O., *The shear strength of a fine sand*, in *Proceedings of the 5th International Conference on Soil Mechanics and Foundation Engineering*, Vol. **1** (Dunod) 1961, pp. 29–37.
[6] Ladd R. S., *Geotech. Test. J.*, **1** (1978) 16.
[7] Lade P. V. and Duncan J. M., *J. Soil Mech. Found. Div., ASCE*, **99** (1973) 793.
[8] Skempton A. W. and Taylor R. N., *Geotechnique*, **4** (1954) 143.
[9] Verdugo R. and Ishihara K., *Soils Found.*, **36** (1996) 81.
[10] Wood D. M., *Soil Behaviour and Critical State Soil Mechanics* (Cambridge University Press) 1990.
[11] Denny P. J., *Powder Technol.*, **127** (2002) 162.
[12] Agnolin I. and Roux J.-N., *Phys. Rev. E*, **76** (2007) 061303.
[13] Finge Z., Doanh T. and Dubujet Ph., *Can. Geotech. J.*, **43** (2006) 1195.
[14] Doanh T., Dubujet Ph. and Protière X., *Acta Geotech.*, **8** (2013) 293.
[15] Castro G., *Liquefaction of sands*, in *Harvard Soil Mechanics Series*, Vol. **81** (Harvard University, Cambridge) 1969.
[16] Benahmed N., Canou J. and Dupla J. C., *C. R. Méc.*, **332** (2004) 887.
[17] Wood D. M. and Lesniewska D., *Granular Matter*, **13** (2011) 395.
[18] Kabla A. and Debrégeas G., *Phys. Rev. Lett.*, **92** (2004) 035501.
[19] Doanh T., Hoang M. T., Roux J.-N. and Dequeker C., *Granular Matter*, **15** (2013) 1.
[20] Adjemian F. and Evesque P., *Int. J. Numer. Anal. Meth. Geomech.*, **28** (2004) 501.
[21] Alshibli K. A. and Roussel L. E., *Int. J. Numer. Anal. Meth. Geomech.*, **30** (2006) 1391.
[22] Nasuno S., Kudrolli A. and Gollub J. P., *Phys. Rev. Lett.*, **79** (1997) 949.
[23] Géminard J. C., Losert W. and Gollub J. P., *Phys. Rev. E*, **59** (1999) 5881.
[24] Tsai J.-C., Voth G. A. and Gollub J. P., *Phys. Rev. Lett.*, **91** (2003) 064301.
[25] Griffa M., Ferdowsi B., Guyer R. A., Daub E. G., Johnson P. A., Marone C. and Carmeliet J., *Phys. Rev. E*, **87** (2013) 012205.